Isı Bilimi ve Tekniği Dergisi, 31, 2, 109-122, 2011
J. of Thermal Science and Technology

ISSN 1300-3615

THE EFFECT OF FIN PITCH ON HEAT TRANSFER AND FLUID FLOW CHARACTERISTICS IN THE ENTRANCE REGION OF A FINNED CONCENTRIC PASSAGE

Kemal KUVVET[*] and Tahir YAVUZ[**]
*Gümüşhane University, Department of Mechanical Engineering,
29100 Gümüşhane, Turkey, kemalkuvvet@hotmail.com
**Başkent University, Department of Mechanical Engineering,
06530 Ankara/Turkey, tyavuz@baskent.edu.tr

(Geliş Tarihi: 18. 05. 2010, Kabul Tarihi: 04. 11. 2010)

Abstract: In this study, the heat transfer and fluid flow characteristics in the unfinned and internally finned concentric passage (smooth and finned annulus) are investigated experimentally. The turbulence characteristics, mean flow, pressure drop and heat-transfer parameters in the entrance region of a concentric passage of diameter ratio 0.2 are measured. The hot-wire anemometer and the liquid-crystal technique are used for the turbulence and mean flow and the heat transfer measurements, respectively. The finned passage is designed as the fin width (W) of 2 mm, the fin height (H) of 2, 4, 6 and 8 mm and the fin pitch (P) of 20, 30 and 40 mm. Reynolds number ranges from 1.8 .104 to 1.24.105 and from 1.65.104 to 7.65.104 for flow and pressure drop and heat transfer measurements, respectively. Experiments are performed for the smooth and finned concentric passages by varying flow and fin parameters and the effects of the fin pitch are investigated. The developing of fluid flow is analyzed and the variation of turbulence intensity, friction factors, local and mean convective heat transfer coefficients in the smooth and finned concentric passages are obtained. Results obtained in the finned concentric passages are compared with the results of the smooth passage. For the average Nusselt numbers and friction factor, empirical equations are developed. As a result, it is seen that the friction factor in the finned passage increases between 3.61 and 18.05 times while the average Nusselt number augments between 1.36 and 5.23 times on the inner surface and between 1.03 and 1.80 times on the outer surface.
Keywords: Heat transfer, Annular duct flow, Finned concentric passage, Finned surface, Liquid-crystal technique, Turbulence, Double pipe heat exchanger.

KANATÇIK ADIMININ KANATÇIKLI KONSANTRİK PASAJIN GİRİŞ BÖLGESİNDEKİ AKIŞ VE ISI TRANSFERİ KARAKTERİSTİKLERİNE ETKİSİ

Özet : Bu çalışmada, iç yüzeyi kanatçıksız ve kanatçıklı konsantrik pasajdaki (düzgün yüzeyli ve kanatçıklı halka kesitli kanalda) ısı geçişi ve akış karakteristikleri deneysel olarak incelenmektedir. Türbülans karakteristikleri, akış alanı, basınç kayıpları ve ısı geçişi ölçümleri, 0.2 çap oranına sahip konsantrik pasajın giriş bölgesinde gerçekleştirilmektedir. Türbülans ve akış ölçümlerinde kızgın telli anemometre, ısı geçişi ölçümlerinde ise sıvı kristal yöntemi kullanılmaktadır. Kanatçıklı pasajda, kanatçık kalınlığı (W) 2 mm, kanatçık yüksekliği (H) 2, 4, 6 ve 8 mm ve kanatçık adımı (P) 20, 30 ve 40 mm olarak tasarlanmıştır. Reynolds sayısı, akış ve basınç kaybı ölçümlerinde 1.8.104÷1.24.105 aralığında değişirken ısı transferi ölçümlerinde 1.65.104÷7.65.104 aralığında değişmiştir. Deneyler, değişen akış ve kanat parametrelerinde düzgün ve kanatçıklı konsantrik pasajlarda gerçekleştirilmiştir ve kanatçık adımının etkileri incelenmiştir. Düzgün ve kanatçıklı konsantrik pasajlardaki akışın gelişimi analiz edilmiş ve türbülans şiddetinin, sürtünme katsayılarının, yerel ve ortalama ısı geçişi katsayılarının değişimleri elde edilmiştir. Kanatçıklı konsantrik pasajlarda elde edilen sonuçlarla düzgün konsantrik aralıktaki sonuçlarla karşılaştırılmıştır. Ortalama Nusselt sayıları ve sürtünme faktörü için deneysel eşitlikler geliştirilmiştir. Kanatçıklı pasajda ortalama Nusselt sayısı iç yüzeyde 1.36 ile 5.23 kat ve dış yüzeyde 1.03 ile 1.80 kat artarken sürtünme faktörünün 3.61 ile 18.05 kat arttığı görülmüştür.
Anahtar Kelimeler: Isı transferi, Halka kanal akışı, Kanatçıklı eşmerkezli kanal, Kanatçıklı yüzey, Sıvı kristal metodu, Türbülans, Çift borulu ısı değiştirici.

NOMENCLATURE

C	circumference length [m]
C_p	specific heat [J/kgK]
d_1	inner diameter of the concentric passage [m]
d_2	outer diameter of the annular passage [m]
d_e	equivalence diameter, [m]
d_h	hydraulic diameter, (d_2-d_1) [m]

f friction factor
h convective heat transfer coefficient [W/m^{2}K]
H fin height
k thermal conductivity [W/mK]
K thickness of the tube [m]
$\dot{m}$ mass flow rate
Nu Nusselt number in the annulus
P fin pitch
r radial coordinate [m]
Re Reynolds number, $\overline{U}.d_h/\nu$
t time [s]
T temperature [K]
$\bar{U}$ mean flow velocity in the annulus [m/s]
W fin width

Greek symbols

α thermal diffusivity of the specimen [m^2/s]
ν kinematic viscosity [m^2/s]
ρ density [kg/m^3]
∞ ambient temperature

Subscripts

af air fluid
b bulk
f finned
fr free convection
i inner
in inlet
lc liquid crystal
o outer
s smooth
w wall
x axial distance

INTRODUCTION

The concentric passage represents a common geometry employed in a variety of heat transfer systems ranging from a simple heat exchanger to the most complicated reactors. The concentric passage is also basic configuration for the double-pipe heat exchangers. Details of the fluid-flow and heat transfer characteristics are necessary for the optimum design of finned passages for the given constraints of each particular application.

Convective heat transfer enhancement can be achieved by active (requiring external energy input) or passive (no external energy input) means. The using fin, which is a passive technique, is often used in the energy industry for compact heat exchangers to enhance the heat transfer rate because this is relatively inexpensive and it does not require direct application of external power during operation. There have been a great number of the experimental and theoretical study to determine the heat and flow field characteristics in the smooth annuli in the literature; on the contrary, there have been smaller quantity studies relating with the finned concentric passage.

Patankar et al. (1979) presented an analytical model for fully developed turbulent air flow in internally finned tubes and annuli. In this study, continuous longitudinal fins, attached to the annulus inner wall, were considered. The thermal boundary conditions were constant heat flux at the inner surface, while the outer boundary was adiabatic. The results of this study consisted of heat transfer and pressure drop coefficients. Renzoni and Prakash (1990), analyzed steady, laminar and forced convection flow and heat transfer in the entrance region of an internally finned concentric circular annular passage. The variation of incremental pressure drop and the local Nusselt number in the entrance region were presented. Agrawal and Sengupta (1987) obtained laminar flow and heat transfer magnitudes in a finned tube annulus numerically. Pressure drops and heat transfer characteristics were reported in the periodically fully developed region by varying geometric and flow parameters. Hsieh and Lin (1993) conducted an experimental study for laminar entrance flow and heat transfer in finned annuli. The nature of flow and heat transfer in finned annuli was investigated in the different geometric and flow parameters, and flow and thermal field visualization were made to give additional insight into the physical phenomena. Garimella and Christensen (1995, 1995) developed friction factor and Nusselt number correlations in annuli with spirally fluted inner tubes for the laminar, transition and turbulent flow regimes. Braga and Saboya (1999) determined average heat transfer coefficients and friction factors for turbulent flow in annular regions with continuous longitudinal rectangular fins attached to the inner wall. Shim et al. (2000) formulated an analytical model for fully-developed turbulent flow and heat transfer in finned annuli using a modified mixing length turbulence model. Mon and Gross (2004) applied the three dimensional numerical study to investigate the effect of the fin pitch on four-row annular-finned tube bundles in staggered and in-line arrangements. The heat transfer and fluid flow characteristics were predicted using the computational fluid dynamics commercial code of FLUENT. Syed et al. (2007) carried out a numerical simulation of the steady and laminar convection in the thermal entry region of the finned annulus for the case of hydrodynamically fully developed flow. Kakalerras and Targui (2008) studied numerically the heat transfer enhancement in a double pipe heat exchanger by using porous fins attached at the external wall of the inner cylinder. They analyzed the effects of several geometrical, physical and thermal parameters such as fin pitch and height, Darcy number and the thermal conductivity ratio on the structure of the hydrodynamic and thermal fields.

Measuring and predicting the overall or local heat transfer coefficient is one of the most important problems in all systems ranging from simple to most complicated one. Convective heat transfer coefficients are experimentally determined through the enthalpy method, the thin boundary wall approximation method and the conduction solution method. In this study, the liquid-crystal technique, which is a member of the conduction solution techniques and especially preferred for the complicated geometries, is used for heat transfer measurements.

Some liquid crystal materials exhibit beautiful colors with visible spectrum when they are heated to the specified temperature ranges. They can be calibrated accurately with proper care and used as temperature indicators. Ferguson (1968), extensively reviewed the chemical, optical and thermal properties, and techniques important to the thermal mapping for non-destructive material testing. Camci et al. (1992, 1993) developed a new hue capturing technique for the quantitative interpretation of liquid crystal images used in convective heat transfer studies and they applied this technique to the convective heat transfer on the curved surfaces. Camci and Glezer (1997) used liquid crystal as temperature indicators on the rotating surface. Baughn et al. (1994) described a liquid-crystal technique used for measuring local heat transfer coefficients in ducts. In this technique, a heated test section suddenly inserts or attaches to the end of a duct in which the air of ambient temperature flows, or a test section with ambient temperature suddenly inserts or attaches to the end of a duct which has an established temperature and flow. Wierzbowski and Stasiek (2002) described the using of thermochromic liquid crystal technique and true-color image processing system in the heat transfer modeling and applied a heat exchanger element.

The flow development and heat transfer characteristics in the entrance region of a finned annulus, which is met in the practical applications, is a complex problem. The purpose of this study is to present comprehensive knowledge about the flow development and heat transfer characteristics in the entrance region of the finned concentric passage. Furthermore, the effects of the fin pitch on the heat transfer and fluid flow characteristics in the concentric passage are determined. So that, the local and overall convective heat transfer characteristics on the inner and outer surfaces in the entrance region of the smooth and finned concentric passages with d_1/d_2=0.2 are measured by using the microencapsulated liquid crystal for Reynolds number and the fin parameters. The turbulence intensity distributions in the axial and radial directions are obtained by using TSI IFA 100 model constant temperature anemometer with a hot-film probe. Pressure measurements are made with a pressure-transmitter in the conjunction with a TSI Model 157 signal conditioner.

EXPERIMENTAL APPARATUS AND PROCEDURE

Experiments are carried out in the test section of the low-speed and open-type thermal wind tunnel. The exit of the wind tunnel and test section are designed as a concentric passage form as shown Figure 1-a. The test section is constructed by fitting a cylinder (smooth and finned) into a tube. The inner and outer diameters of the tube are 172 mm and 180 mm, respectively, and the tube is made of plexiglas (thermal conductivity=0.1884 W/Km, density=1200 kg/m^3, specific heat=1468.3 J/kgK (Kakaç et al., 1987)) to be able record liquid crystal colors on the concentric passage surfaces (Baughn et al., 1994). The cylinder and fins are constructed of polyamid (thermal conductivity=0.29 W/Km, density=1150 kg/m^3, specific heat=1680.3 J/kgK (KERN, 1995)), which is one of the PVC materials. The diameter of the cylinder is manufactured as 34.4 mm to obtain the radius ratio of 0.2. In the finned concentric passage, the fins are constructed very tightly on the outer surface of the inner cylinder for the different fin pitch.

In order to obtain the pressure drop and then the friction factor, 46 static pressure taps are installed through the plexiglas tube. The taps are placed firstly after 30 mm from the entrance of the test section and then each 10 mm locations. For the measurements of the velocity and turbulence, three tapping holes are carried on the outer tube of test section for crossing the hot-wire probe and supported. The first hole is opened at the $x/d_h \cong 0$ position (at the end of the wind tunnel and before the 20 mm of the test section) and the others are opened at the x/d_h=1.817 and 3.416 positions. A schematic diagram of the overall apparatus used in the present study and test section are shown in Figure 1.

The air is taken into the wind tunnel by the centrifugal fan operated with a speed control unit. It is then passed through a 24 kW heater which is operated by a digital heater controller. The controller was produced by OMRON Company as E5CK model. After the heater, the air flow is passed through the settling chamber with the honeycomb flow straighteners and the constriction (see Fig. 1), respectively, and then enters the test section with almost uniform velocity and temperature profiles. The flow rates are controlled with a speed control unit by taking into account the static pressure difference at the wind tunnel exit between I and II positions (see Fig. 1). A pressure transmitter belongs to MODUS Instruments Company with T30 serial number is used to measure the static pressure differences.

The velocity and the pressure measurements are carried out by using a computer-controlled data acquisition system. For the velocity measurements at the three axial positions (x/d_h=0, 1.817, 3.416) and 11 radial positions, 2048 data are acquired at a sampling rate of 1 kHz using low-pass filter setting of 300 Hz. So, the measuring time correspondes to 2.0486 s. The pressure signals are acquired at a rate of 200 sample/sec and low-pass filtered at 100 Hz. Each of the mean pressure is obtained by means of integrating the time history of 2048 data for over 10 s. TSI Thermal-Pro Software is used to acquire signals with a 12-bit A/D converter and obtains the statistical results of these signals. The experimental uncertainties in the measurement of the velocity and pressure are determined to be less than ±3.2% and ±3.1%, respectively.

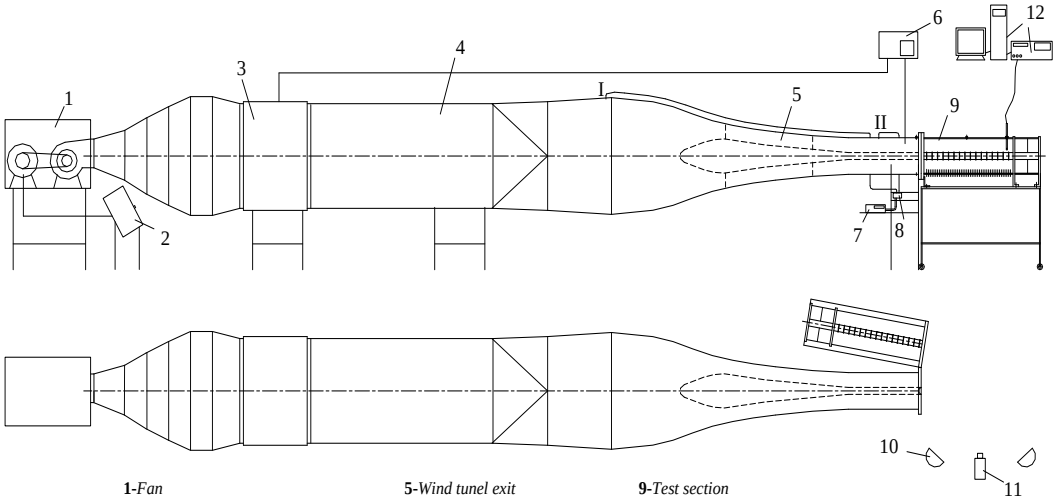

1-*Fan*
2-*Speed control unit*
3-*Heater*
4-*Settling chamber and construction*
5-*Wind tunel exit*
6-*Heater control unit*
7-*Multimeter*
8-*Pressure transmitter*
9-*Test section*
10-*Lights*
11-*Camera*
12-*Computur, anemometer, hot-film probe*

a-*Experimental setup*

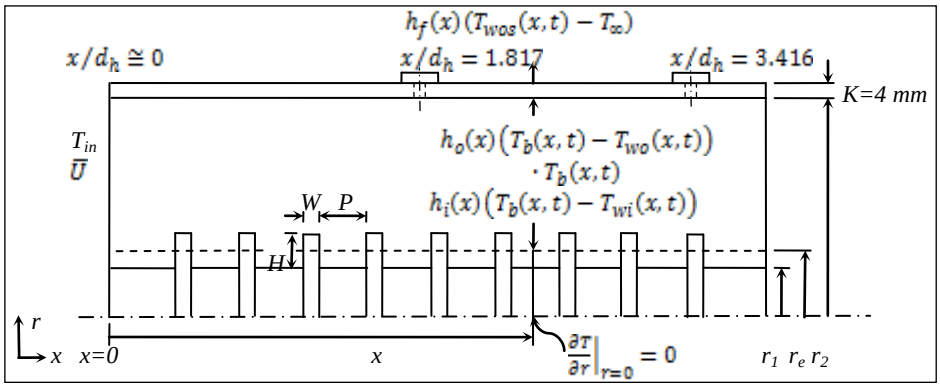

b-*Test section and boundary conditions used heat transfer calculation*

Figure 1. Schematic diagram of experimental apparatus and test section.

The insertion technique using the transient method with liquid crystals is used for measuring local convective heat transfer coefficients on the inner and outer surfaces of the concentric passage. Before the heat transfer measurements, the liquid crystal used in the experiments is calibrated. A water bath and a copper plate are used as the calibration devices. For obtaining very good liquid crystal colors, a thin layer of black paint being ink form is air brushed on the surfaces of the concentric passage and the copper plate, and then the liquid crystal is air brushed on top of the black paint (Fergason, 1968; Baughn et al., 1994).

During the calibration, the water is heated electrically and its temperature and the color of the liquid crystal layer on the copper plate are recorded by a video camera. The output of the camera is watched several times by using a video recorder and TV. In this way, the generation temperature of the liquid crystal colors are determined and given in Table 1.

The green color is used for the reference temperature (T_{lc}: the liquid crystal transition temperature) in this experimental works, due to its brightness and clarity on the video display and its narrow bandwidth. From the calibration, the green color corresponds to a change temperature of 42.1°C and color bandwidth of 0.6 °C. The experimental uncertainty in the measurement of T_{lc} is determined to be less than ±2.8%.

Table 1. The generation temperature of the liquid crystal colors

Color	Temperature (°C)	Color Bandwidth (°C)	Average Color Temperature (°C)
Red	40.9 – 41.8	0.9	41.35
Green	41.8 – 42.4	0.6	42.10
Blue	42.4 – 45.6	3.2	44.00

The measurements of the heat transfer characteristics are carried out in two parts. In the first part, after preheating the wind tunnel to the desired temperature (60±0.2°C), the test section is suddenly inserted and attached with the exit of the wind tunnel. The position

and the generation time of the liquid crystal transition color (green color) on the concentric surfaces, as shown in Figure 2, are obtained by using a video camera and chronometer. For observing the liquid crystal colors on the surfaces, the layer of the black paint and liquid crystal on the outer surface of the passage is constituted as 1,2 cm width.

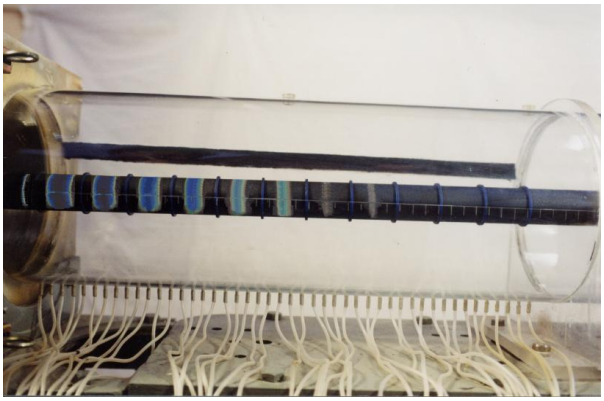

Figure 2. Typical liquid crystal display on the concentric surfaces

In the second part, the local and mean heat transfer characteristics are calculated by using the values of the position and the generation time of the liquid crystal transition color and solving the energy balance equations for the smooth or finned inner cylinder and the thickness of the outer tube of the concentric passage.

For the finned cylinder, the diameter of equivalence cylinder, d_e is defined as;

$$d_e = 2\,r_e = 2\,(r_1 + (H^2 + (2\,r_1 + W)\,H)/P) \qquad (1)$$

and assuming negligible heat transfer in the axial direction and circumferential direction because of d_e being very small than the length of the test section and the symmetry, the general transient heat conduction equation in cylindrical polar coordinates, the initial and boundary conditions (referring Figure 1-b) are expressed as,

$$\frac{\partial^2 T}{\partial r^2} + \frac{1}{r}\frac{\partial T}{\partial r} = \frac{1}{\alpha_i}\frac{\partial T}{\partial t};\ 0 \le r \le r_e,\ t > 0 \qquad (2)$$

$$T(r) = T_\infty;\qquad 0 \le r \le r_e, t = 0 \qquad (3)$$

$$\frac{\partial T}{\partial r} = 0,\qquad r = 0,\ t > 0 \qquad (4)$$

$$k_i \frac{\partial T}{\partial r} = h_i(x)\left(T_b(x,t) - T_{wi}(x,t)\right);\ r = r_e, t > 0 \qquad (5)$$

For the thickness of the outer tube, since it has a low thermal diffusivity and its thickness is very small than the test section's length, the general transient heat conduction equation in cylindrical polar coordinates is defined;

$$\frac{\partial^2 T}{\partial r^2} + \frac{1}{r}\frac{\partial T}{\partial r} = \frac{1}{\alpha_o}\frac{\partial T}{\partial t};\ r_2 \le r \le r_2 + K,\ t > 0 \qquad (6)$$

and the initial and boundary conditions (referring Figure 1-b) are expressed as,

$$T(r) = T_\infty;\ r_2 \le r \le r_2 + K,\ t = 0 \qquad (7)$$

$$k_o \frac{\partial T}{\partial r} = h_o(x)\left(T_b(x,t) - T_{wo}(x,t)\right);\ r = r_2, t > 0 \qquad (8)$$

$$k_o \frac{\partial T}{\partial r} = h_{fr}(x)\,(T_{wos}(x,t) - T_\infty);\ r = r_2 + K, t > 0 \qquad (9)$$

where $\alpha_i\left(= k_i/(\rho_i C_{p,i})\right)$ and $\alpha_o\left(= k_o/(\rho_o C_{p,o})\right)$ are the thermal diffusivities of the inner cylinder (polyamid) and the outer tube (plexiglas), respectively; t is time; r and x are the radial and axial coordinates; K is the thickness of the outer tube; $T_{wos}(x,t)$ is the surface temperature of the outer tube; $h_{fr}(x)$ is the average free convection coefficient at the outer wall of the tube and $T_b(x,t)$ is the local fluid bulk temperature into the concentric passage at the x position. $h_{fr}(x)$ is estimated by using the correlation formula in the literature (Churchill and Chu, 1975).

The local fluid bulk temperature, $T_b\,(x,t)$, is obtained by iteration because it depends on the upstream convective heat transfer coefficients. It is calculated by using the energy balance on a local circumferential section of the concentric duct;

$$\dot{m}\,C_{p,af}\,dT_b(x,t) = C_i\,h_i(x)\,[T_b(x,t) - T_{wi}(x,t)]\,dx + C_o\,h_o(x)\,[T_b(x,t) - T_{wo}(x,t)]\,dx \qquad (10)$$

For the every time (t), $T_b(x,t)$ is obtained by integrating Eq. (10) from the inlet of the test section, $x_0=0$, to the local position given by x_n

$$T_b(x,t) = T_{in} - \frac{C_i}{\dot{m}\,C_{p,af}}\int_{x_0}^{x_n} h_i(\varphi)[T_b(\varphi,t) - T_{wi}(\varphi,t)]d\varphi - \frac{C_o}{\dot{m}\,C_{p,af}}\int_{x_0}^{x_n} h_0(\varphi)[T_b(\varphi,t) - T_{wo}(\varphi,t)]d\varphi \qquad (11)$$

In this equation, C_i and C_o are the circumference length of the inner and outer surface of the concentric passage, respectively; $C_{p,af}$ is the specific heat of the fluid at $\left(T_{in} + T_b(x,t)\right)/2$ temperature. During an experiment, the inlet temperature in the test section, $T_{in} = 60 \pm 0.2$℃, is kept constant by digital heater controller, while the wall temperatures (T_{wi}, T_{wo}) rise from T_∞ to T_{lc}.

The differential equations are replaced using the implicit finite difference approximation, the energy transfer methods and the boundary conditions and then the nodal equations are developed and solved by using Thomas Algorithm. At the start of calculations, the initial values of the convective heat transfer coefficients $(h_i(x),\ h_o(x))$ are set very small. After the iteration, the wall node temperatures $(T_{wi}(x), T_{wo}(x))$ are compared with the change temperature of the liquid crystal (T_{lc}). If the wall node temperatures calculated are at a lower or higher temperature then T_{lc}, hence the value of the convective heat transfer coefficients of the surfaces are increased or decreased according to the

magnitude at the differences of the two temperatures $((T_{lc} - T_{wi}(x)$ and $(T_{lc} - T_{wo}(x))$. The calculation procedure repeates until the difference is less than 0.01°C. Afterwards, the local Nusselt numbers of the concentric surfaces are calculated using the hydraulic diameter (d_{he}) as a characteristic length defined as $d_{he}=d_2-d_e$, the thermal conductivity of air (k_{af}) , which is evaluated at $(T_{lc} + T_\infty)/2$ temperature, the local convective heat transfer coefficients $(h_i(x), h_o(x))$ and Eq. (12);

$$Nu_{xi}(x) = h_i(x)\frac{d_{he}}{k_{af}} \quad , \quad Nu_{xo}(x) = h_o(x)\frac{d_{he}}{k_{af}} \qquad (12)$$

The whole procedure is repeated for the number of reading and then the Nusselt number distributions along the concentric passages are obtained. The detail of the experimental and calculation procedures can be found in Kuvvet (2002).

RESULTS AND DISCUSSION

The flow field characteristics are determined at the cold wind tunnel (the heater turned off) by using the hot-film anemometer and a pressure transmitter. The radial distributions of the axial velocity component at x/d_h=0, 1.817 and 3.416 positions for P=20 mm are shown in Figure 3. As shown in Figure 3, while the velocity profiles are uniform at the inlet of the test section, the velocity gradients on the inner and outer surfaces of the concentric passage and at the points of the maximum velocity increase trough the axial direction. The location of the maximum velocity tends to the outer surface of the concentric passage with using fin. Both the values of the velocity gradients and the radial distance of the maximum axial velocity component increase with fin height. The maximum velocity moves to the inner surface trough the exit of the test section.

The variations of the axial velocity component at the exit of the test section are shown in Figure 3 and Figure 4 for the different fin pitch. These figures has shown that the velocity gradient and the maximum velocity distance decrease with the fin pitch for H=2 mm but increase for H≥4 mm in the finned passage. For H=2 mm, while the axial velocity component is maximum approximately at r^*=0.58 point for P=20 mm, it is maximum nearly at r^*=0.53 for P=40 mm. For H=8 mm, it is maximum at r^*=0.64 and 0.68 for the fin pitch of 20 mm and 40 mm, respectively. It has been concluded that the flow has separated from the inner surface by the fins and reattached to the surface before the following fins for the low fin heights but not reattached to the inner surface and separated again for the high fin heights.

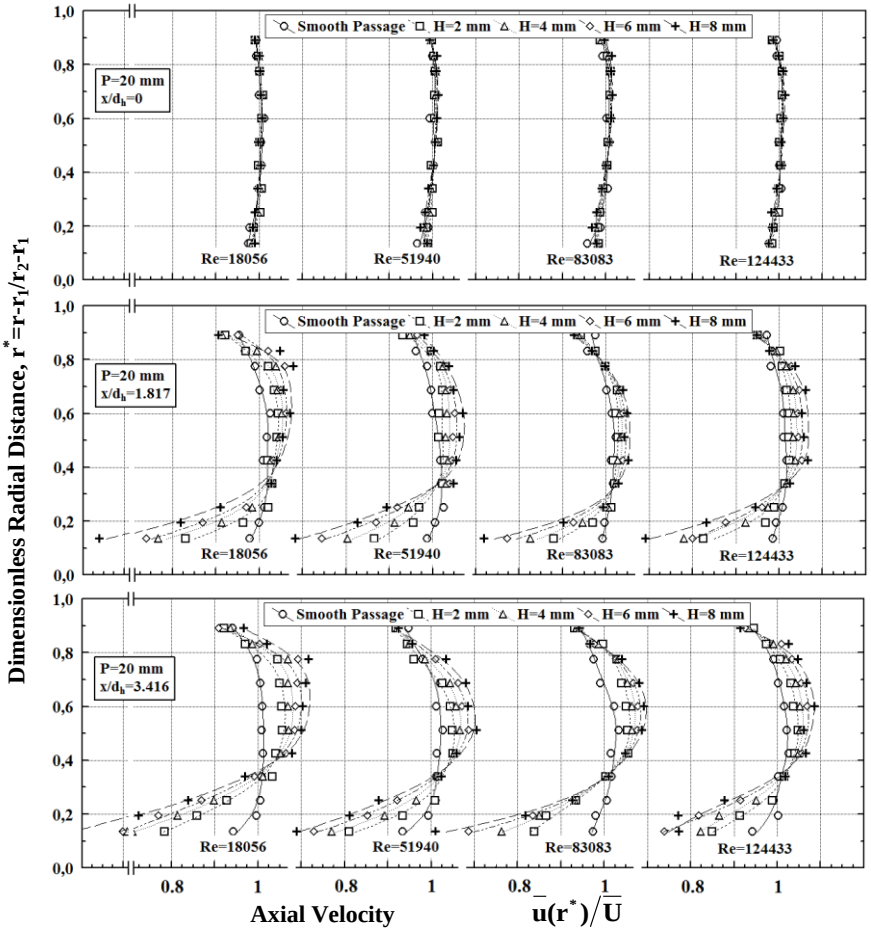

Figure 3. Variation of axial velocity component for P=20 mm and different x/d_h, Re, H.

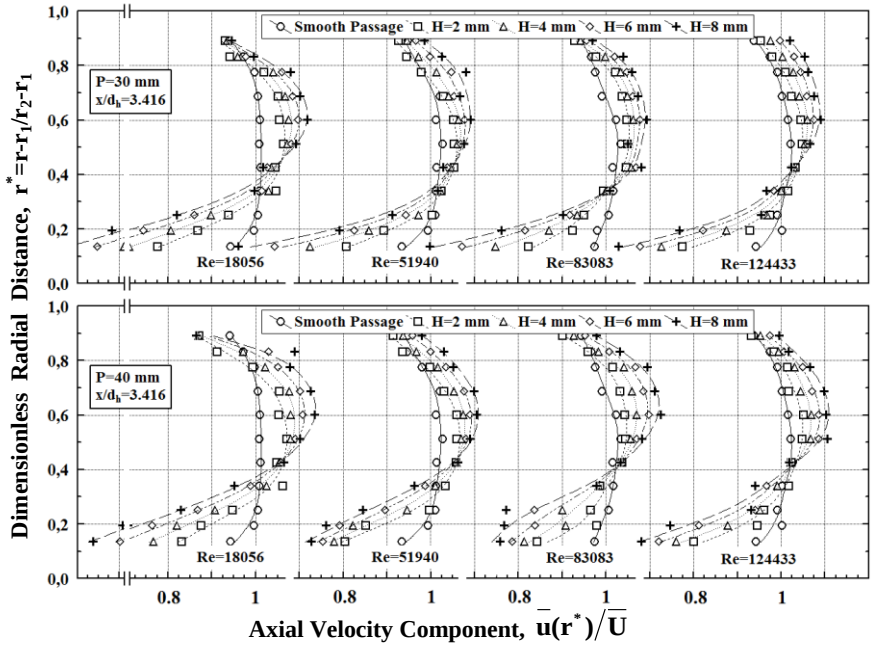

Figure 4. Variation of axial velocity component for the different fin pitch at the exit of the test section.

In order to obtain the pressure drops and then the friction factors, the static pressure taps installed along the plexiglas tube (the outer surface of annuli) are used.

The friction factor is denoted as

$$f_x = \frac{(\Delta P/x)\, d_h}{\rho \cdot \overline{U}^2/2} \qquad (13)$$

where, $\Delta P = P_0 - P_x$ is the pressure drop (P_0: the pressure at the inlet of the test section (the exit of the wind tunnel), P_x: the pressure at the x position of the test section); ρ is the air density at the ambient temperature; $\overline{U}$ is the axial average velocity obtained by using axial velocity distributions at the inlet of the test section. ΔP is measured between 40 mm (P=20 mm and P=40 mm) and 30 mm distances (P=30 mm) in the test section.

Figures 5 and 6 present the variation of the local friction factors along the downstream distance for the smooth and finned concentric passages. The local friction factors are obtained for H=2 mm and H=8 mm at various Reynolds numbers and fin pitch. As expected, the friction factors for the finned passage are much higher than the corresponding results for the case of the smooth passage. All the local friction factors decrease with Reynolds number and logarithmically along the downstream direction. As shown in Figures 5 and 6, while the friction factors go down with P for H=2 mm, they go up with P for H=8 mm.

By taking into consideration the total pressure drop at the test section, the average friction factors for the smooth and finned passages are obtained. For calculating of these values with Eq.(13), the static pressures at the inlet and outlet of the test section (ΔP=P0-P46) and the distance of these points (x0-x46 =L=500 mm) are considered. Figure 7 shows the

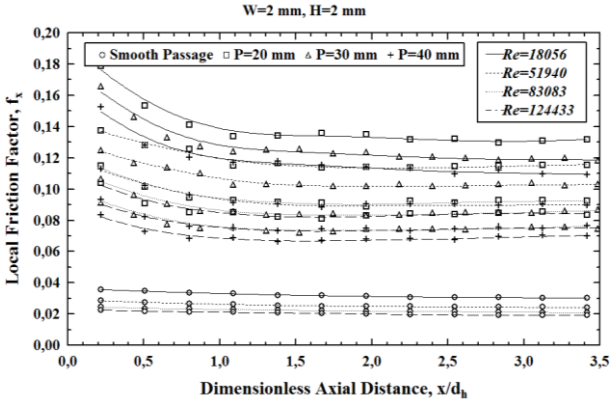

Figure 5. Local friction factor distribution with different Re and P values along the downstream distance for H=2 mm.

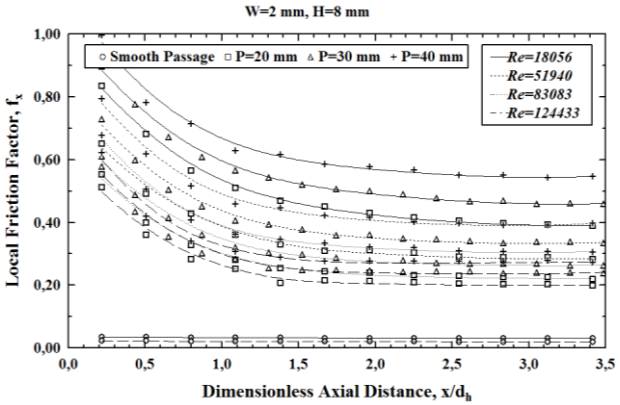

Figure 6. Local friction factor distribution with different Re and P values along the downstream distance for H=8 mm.

average friction factors versus Reynolds number for the smooth and finned concentric passages. It can be seen from Fig. 7 that the friction factors in the finned passage decrease with the Reynolds number but increase with the fin height. Furthermore, as seen in the changes of the local friction factor, the average friction factors in

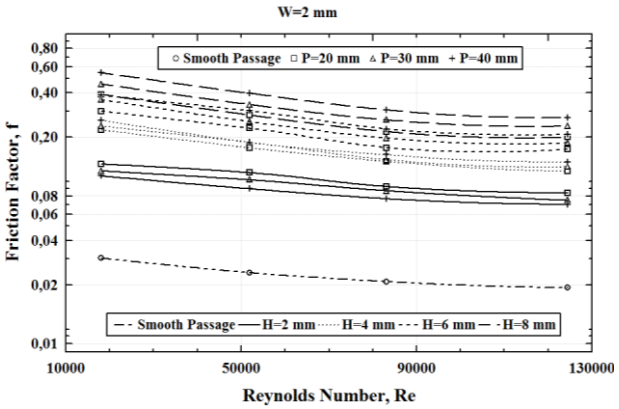

Figure 7. Friction factor versus Reynolds number for smooth and finned concentric passage.

the test section diminish with P at H=2 mm but they rise for H ≥4 mm. The increment ratios of the friction factor with the fin pitch go up with the fin height for H ≥4 mm. The friction factor in the finned passage increases between 3.61 and 18.05 times because of the using fin. The uncertainty for the friction factors is estimated as ±7.9%.

The changes of turbulence intensities with the fin parameters and Reynolds number are shown in Figures 8-10. As can be seen from these graphs, while the turbulence intensities on the inner surface are smaller than the values on the outer surface in the smooth passage, they are greater than the ones on the outer surface in the finned passage. They are higher in the regions of the inner and outer concentric surfaces and increase with the fin height. Besides, the axial turbulence intensities are greater than the radial values. In all cases, the minimum turbulence intensities occur at the maximum velocity points. As Reynolds number increases, turbulence intensities in the regions near the surface go down, whereas they go up close to the maximum velocity locations.

Figure 8 shows the distributions of the axial and radial turbulence intensities at the inlet and exit of the test section in the smooth and finned passages for P=20 mm and Re=18056. As shown in Fig. 8, while the turbulence intensities at the inlet are close each other and low values, they increase at the exit of the test section on the surfaces but decrease at the maximum velocity regions due to the use of fins. Through the axial direction in the finned passage, the increases in the radial turbulence intensity are greater than the axial ones.

Figure 9 represents the turbulence intensity distributions at the exit of the test section and Re=18056 for the different fin pitch. It can be seen from Figs. 8 and 9 that the turbulence intensities decrease with P for H=2 mm but increase with P for H≥4 mm. This situation usually occurs on the inner surface. The difference between the turbulence intensities at the different fin heights decreases from the inner surface to the minimum turbulence intensity points at the radial direction. After these points, there are no significant differences.

For the different fin pitch, the turbulence intensity distributions at Re=124433 and x/d_h=3.416 are given in Figure 10. As shown in this figure, similar changes are obtained at the high Reynolds number for the turbulence intensities. But, their values reduce with the Reynolds number.

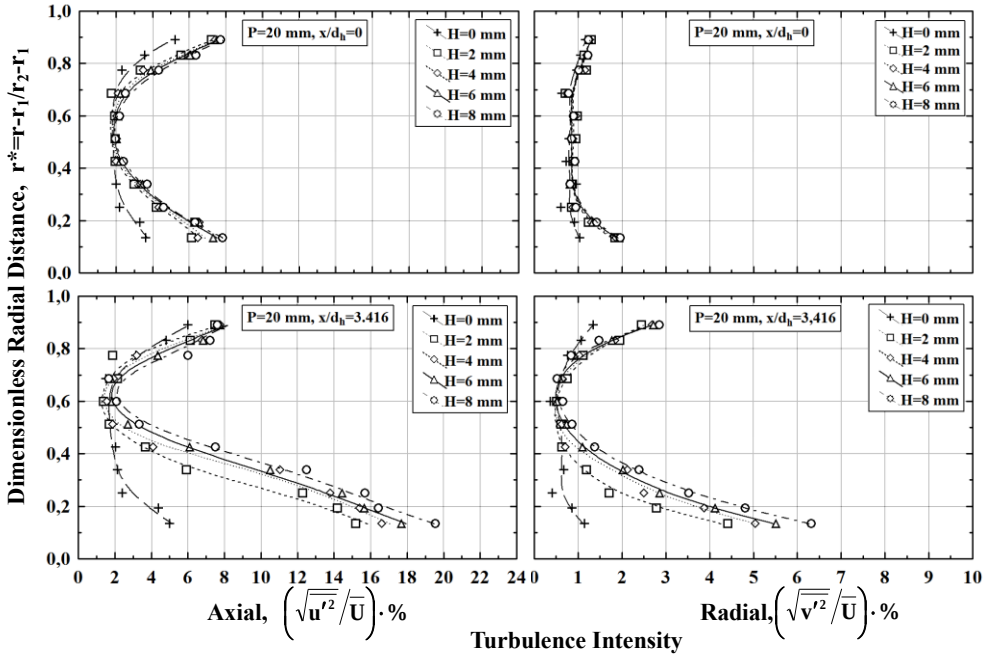

Figure 8. Turbulence intensity distribution for different H and x/d_h at P=20 mm and Re=18056.

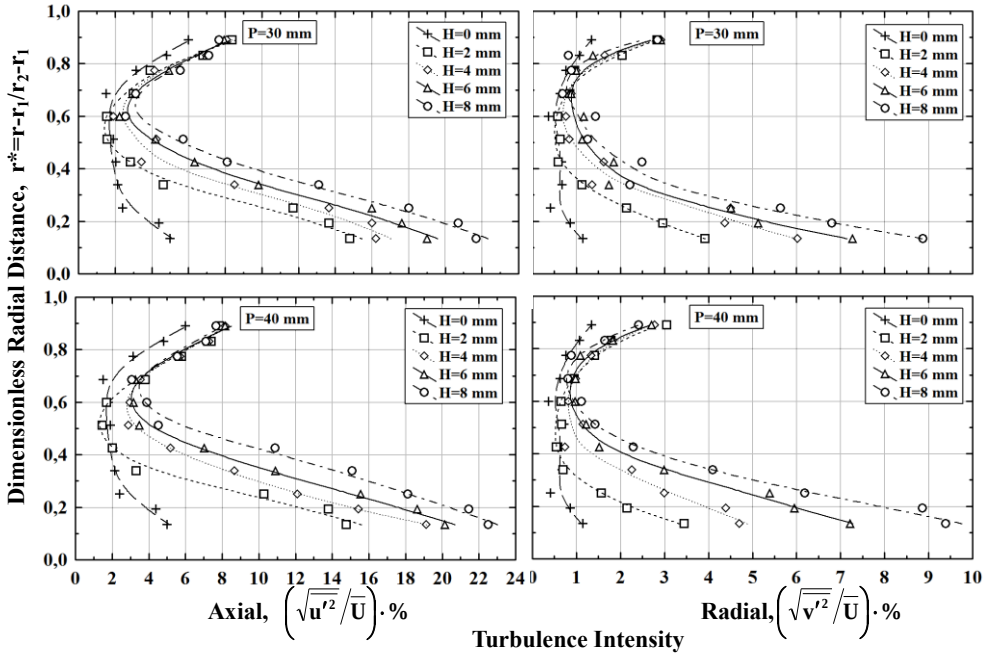

Figure 9. Turbulence intensity distributions for different H and P at x/d_h=3.416 and Re=18056.

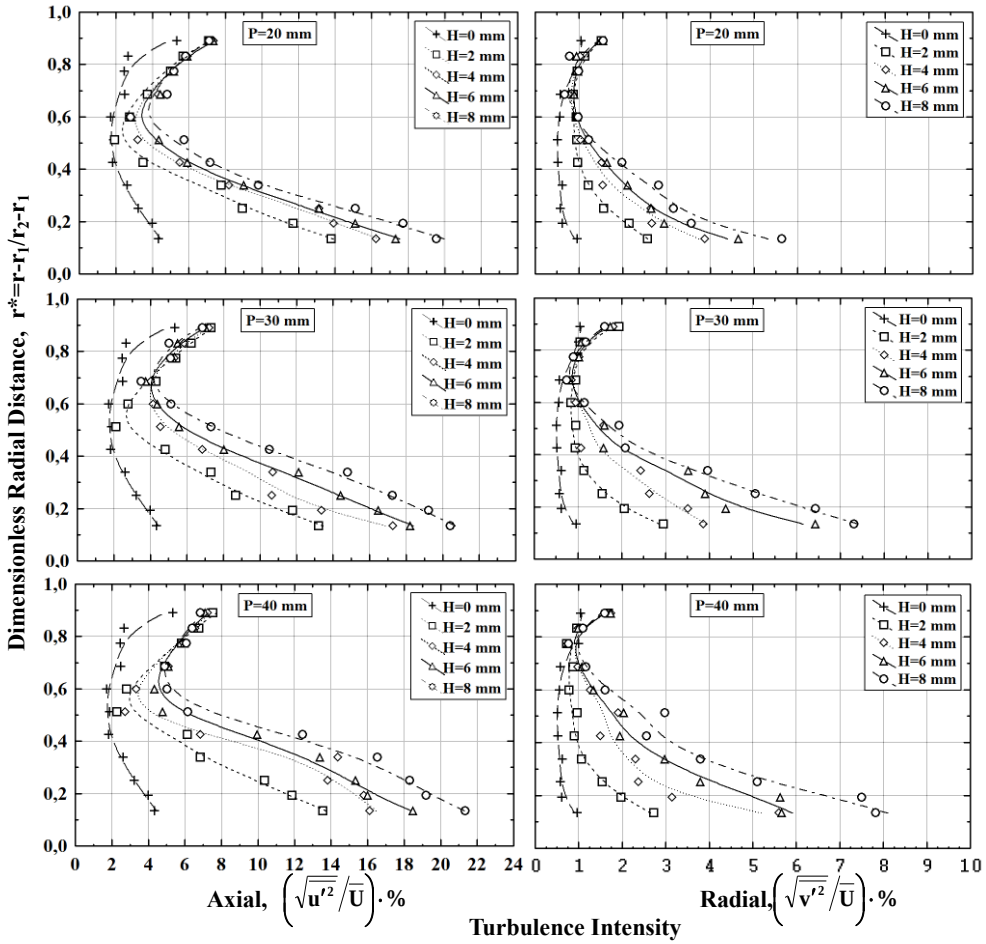

Figure 10. Turbulence intensity distributions for different H and P at x/d_h=3.416 and Re=124433.

The local Nusselt numbers (Nu_{xis}, Nu_{xos}) versus the axial distance along the inner and outer surface of the smooth concentric passages at the different Reynolds numbers are presented in Figure 11. Due to the insufficiency of the wind tunnel heater, the heat transfer measurements were carried out for the lowest three flow rates. The local convective heat transfer coefficients ($h_i(x)$, $h_o(x)$) were calculated for every 5 cm through the test section. As shown in Fig. 11, the local Nusselt numbers on the inner surface are higher than those on

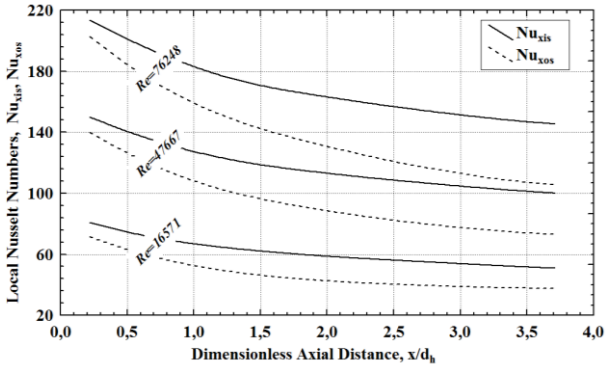

Figure 11. Local Nusselt number distribution for the smooth concentric passage.

the outer surface. Nu_{xis} and Nu_{xos} decrease logarithmically along the entrance region of the smooth passage and increase with Reynolds numbers.

The variations of the local Nusselt numbers normalized with the values of the smooth passage in the finned passage are presented in Figures 12 and 13. In general, the convection rates on the top of the fins are significantly higher than those on the floor which is placed between the fins for all the Reynolds numbers and the fin configurations. The minimum heat transfer rate on the finned surface occurs at the backside of the fins. The flow separates from the inner surface by the fins and reattaches to the surface before the following fins for the low fin heights. But, for the high fin heights, it cannot reattach to the surface before the following fins and it separates again. The heat transfer rate has maximum value at the reattachment point between two fins for the low fin heights and decreases toward the fins. For the high fin heights, the maximum heat transfer occurs near the second fin and decreases towards the first fin in the fin spaces.

The heat transfer develops differently in the smooth and finned passages. While the fully developed conditions can not been reached in the smooth passage, they are nearly reached in the finned passage. The variation of the local values is too small on the inner concentric surface after a few periods from the entrance. In the finned passage, the local Nusselt numbers increase because of the turbulence and the expansion of the heat transfer surface. At the exit of the test section, the local Nusselt numbers rise between 1.2 and 6.3 times on the inner surface and between 1.02 and 2.12 times on the outer surface.

As shown in Figs. 12 and 13, the thermal entrance length increases with P and Re and decreases with H. In spite of the increasing of the turbulence intensity, the increment ratio in the local Nusselt numbers goes down with P because of the smaller heat transfer surface. Also, this ratio diminishes with Re, as shown in Fig. 14.

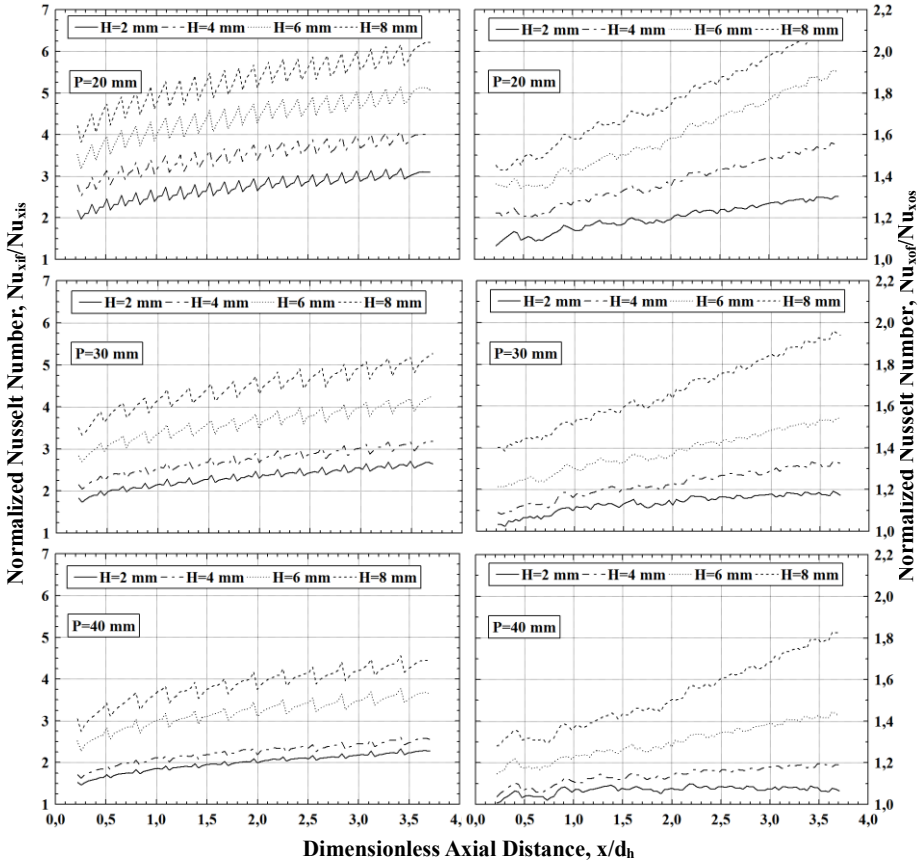

Figure 12. Normalized Nu distribution in the finned concentric passage at Re=16571.

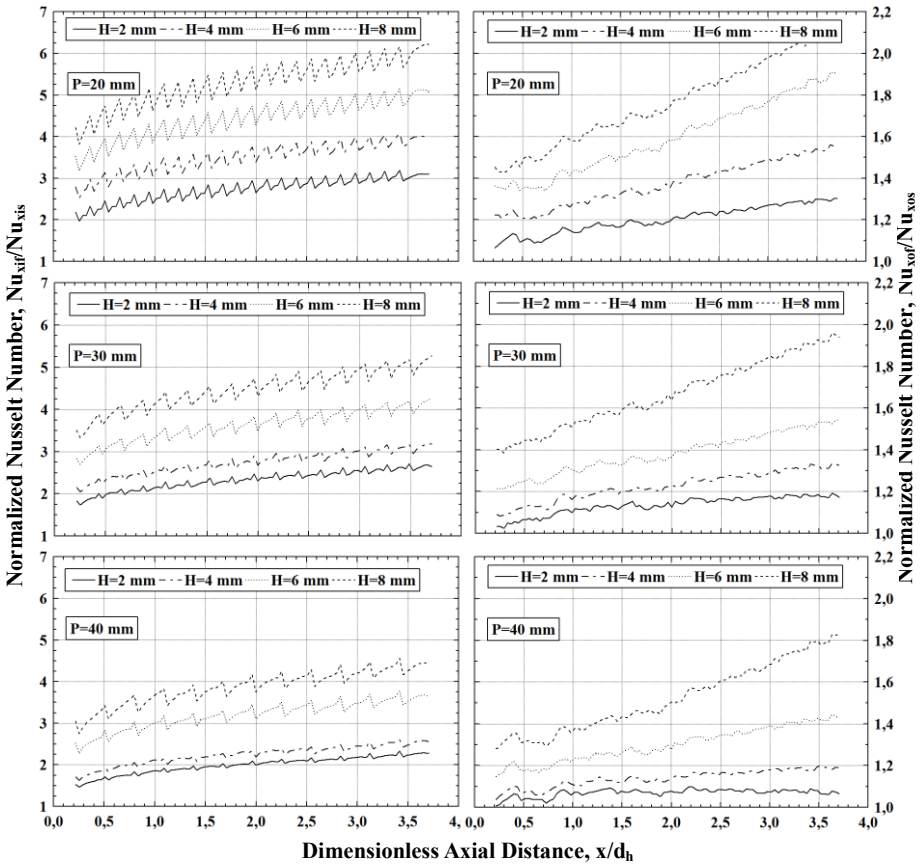

Figure 13. Normalized Nu distribution in the finned concentric passage at Re=16571.

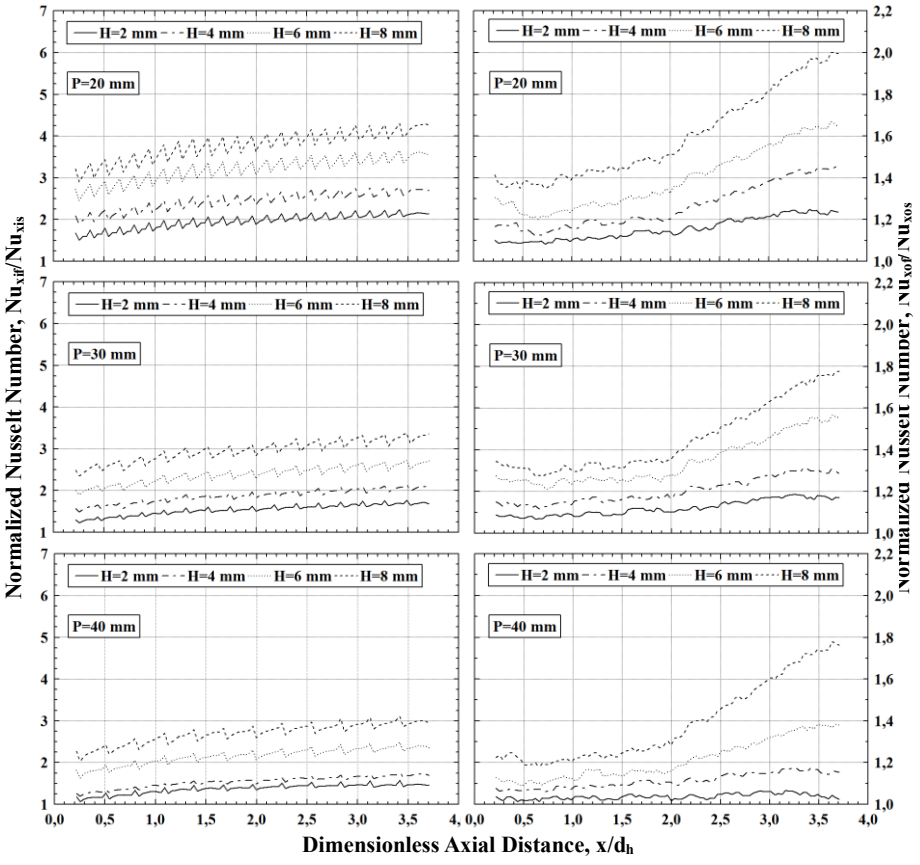

Figure 14. Normalized Nu distribution in the finned concentric passage at Re=76248.

By using the local Nusselt number variations on the surfaces of the smooth and finned passages, the average Nusselt numbers at the test section are calculated numerically by Eq.(14). For the different fin parameters and Re, the average Nusselt numbers are presented in Fig. 15. For the average Nusselt numbers on the inner and outer concentric surfaces, the total uncertainties are estimated as ±5.9% and ±4.9%, respectively.

$$\overline{Nu}_i = \frac{1}{x_n - x_1}\int_{x_1}^{x_n} Nu_{xi}(x)\,dx$$
$$\overline{Nu}_o = \frac{1}{x_n - x_1}\int_{x_1}^{x_n} Nu_{xo}(x)\,dx \qquad (14)$$

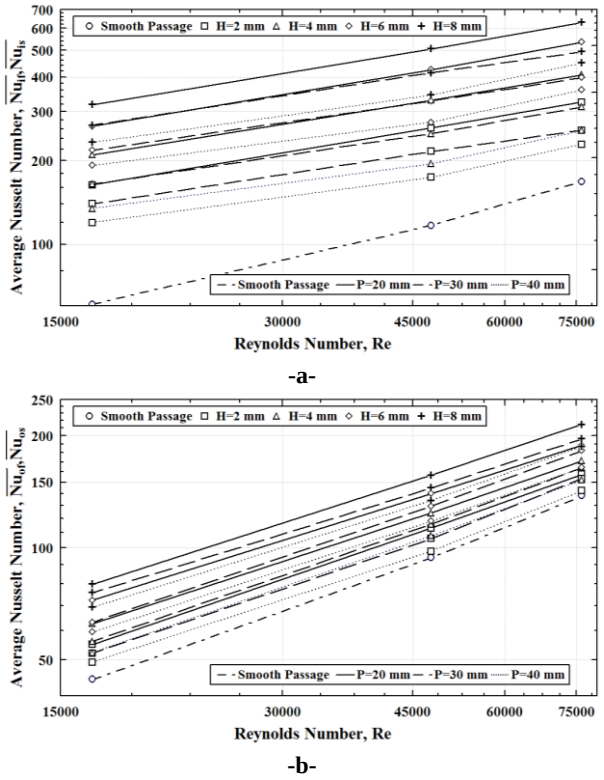

Figure 15. Average Nusselt numbers on the inner (a) and outer (b) concentric surfaces.

The effects of the fin pitch, the fin height and Reynolds number on the heat transfer are given in Figure 15. It seems that the increasing ratios of the Nusselt numbers decrease with the Reynolds number and these ratios are grater on the inner surface than those on the outer surface. The increment ratios of the average Nusselt numbers at Re=16571 change between 1.97 and 5.23 on the inner surface and between 1.11 and 1.80 on the outer surface. On the other hand, those ratios at Re=76248 change between 1.36 and 3.74 on the inner surface and between 1.03 and 1.56 on the outer surface.

Finally, some empirical equations have been developed for f, $\overline{Nu_i}$, $\overline{Nu_o}$ by using experimental results and least squares method. Eq. (15), which is similar to that used Garimella and Christense (1995) for spirally enhanced geometries, is obtained for the friction factor with a maximum error of ±%7,3. This correlation is valid for W=2 mm, 20 mm≤P≤40 mm, 2 mm≤H≤8 mm and 18000≤Re≤125000. The results of measured and predicted friction factors are compared in Fig. 16-a.

$$f_f = f_s\left[1 + 762{,}04\, Re^{-0{,}0866}\left(\frac{P}{d_h}\right)^{0{,}186}\left(\frac{H}{d_h}\right)^{1{,}013}\right] \qquad (15)$$

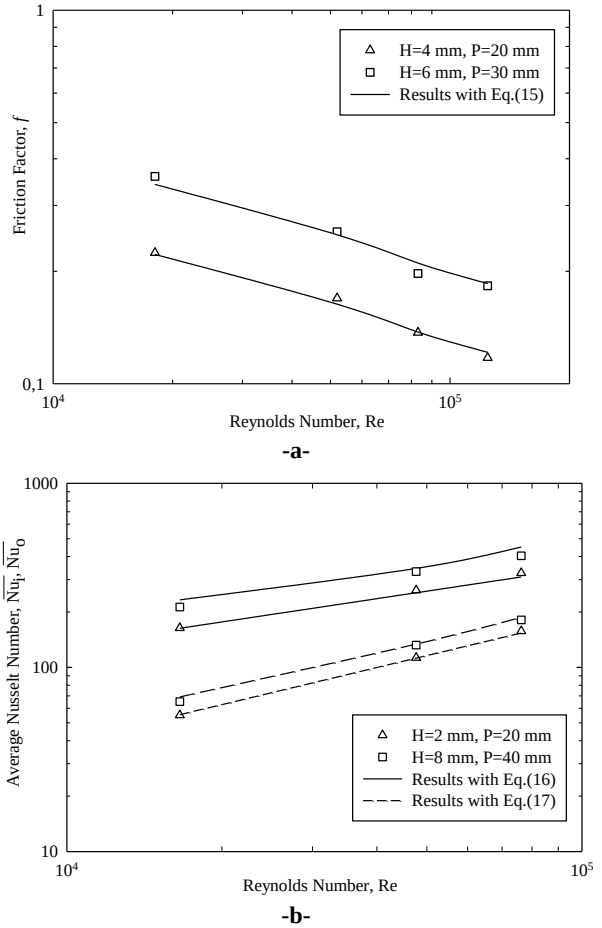

Figure 16. Measured and predicted values: **a-**friction factor **b-**average Nusselt numbers.

For the average Nusselt numbers, Eq. (16) and Eq. (17) are correlated in terms of Re and dimensionless fin parameters. Although the fluid used in the experiments is air (Pr=0,707 at the temperature of $(T_{ic} + T_\infty)/2 \cong 32°C$), these equations are possible, as suggested Patankar et al. (1979), to generalize the results for other fluids by introducing the factor $Pr^{0,4}$. The Eq. (16) and Eq. (17) have been obtained with the maximum errors of ±%4,7 and ±%3,1 respectively and are valid for the above fin parameters and 16500≤Re≤75000. Measured and predicted average Nusselts numbers have been compared in Fig. 16-b and good agreement has been obtained.

$$\frac{\overline{Nu_i}}{Pr^{0,4}} = 7{,}917.Re^{0,42}.\left(\frac{P}{d_h}\right)^{-0{,}565}\left(\frac{H}{d_h}\right)^{0{,}474} \qquad (16)$$

$$\frac{\overline{Nu_o}}{Pr^{0,4}} = 0{,}1638.Re^{0{,}669}.\left(\frac{P}{d_h}\right)^{-0{,}206}\left(\frac{H}{d_h}\right)^{0{,}221} \qquad (17)$$

CONCLUSIONS

The flow and heat transfer characteristics in the entrance region of the smooth and finned concentric passages for the diameter ratio of 0.2 are investigated experimentally. At the end of the study, the following results are obtained:

i) The location of the maximum velocity in the finned passage tends to the outer surface and its radial distance decreases with the fin pitch for H=2 mm but increases for H≥4 mm.

ii) The friction factors in the test section decrease with P at H=2 mm but they increase with P for H ≥4 mm. The increment ratios of the friction factor with the fin pitch go up at the high fin height.

iii) The minimum turbulence intensities in the finned passage occur at the maximum velocity points. The turbulence intensities increase with the fin height and decrease with Reynolds number. The turbulence intensities diminish with P for H=2 mm but rise with P for H≥4 mm. The axial turbulence intensities are greater than the radial values.

iv) In the finned concentric passage, the maximum heat transfer occurs on the top of the fin and the minimum heat transfer occurs at the backside of the fin.

v) In spite of the increasing in the turbulence intensity, the increment ratio in the local Nusselt numbers goes down with P because of the smaller heat transfer surface and with Reynolds number because of the decreasing turbulence intensity.

REFERENCES

Agrawal, A.K., Sengupta, S., Laminar flow and Heat Transfer in a Finned Tube Annulus, *Int.J. Heat and Fluid Flow* 11 (1), 54-59, 1990.

Baughn, J.W., Yan, X., Roby, J.L., An Insertion Technique Using the Transient Method with Liquid Crystals For Enhanced Heat Transfer Measurements in Ducts, *Enhanced Heat Transfer* 1, 179-190, 1994.

Braga, C.V.M., Saboya, F.E.M., Turbulent Heat Transfer, Pressure Drop and Fin Efficiency in Annular Regions with Continuous Longitudinal Rectangular Fins, *Experimental Thermal and Fluid Science* 20, 55-65, 1999.

Camci, C. and Glezer, B. Liquid Crystal Thermography On The Fluid Solid Interface Of Rotating Systems, *Transactions ASME* 119, 20-29, 1997.

Camci, C., Kim, K. and Hippensteele, S. A. A New Hue Capturing Technique for the Quantitative Interpretation of Liquid Crystal Images Used In Convective Heat Transfer Studies, *ASME J. Turbomachinery* 114, 765-775, 1992.

Camci, C., Kim, K., Hippensteele, S. A. and Poinsatte, P. E. Evaluation Of A Hue Capturing Based Transient Liquid Crystal Method For High Resolution Mapping Of Convective Heat Transfer On Curved Surfaces, *ASME J. Heat Transfer* 115, 311-318, 1993.

Churchill, S.W., Chu, H.H.S., Corelating Equations for Laminar and Turbulent Free Convection from a Horizantal Cylinder, *Int.J. Heat Mass Transfer* 18, 1049-1053, 1975.

Fergason, J. L. Liquid Crystals in Nondestructive Testing, *Applied Optics* 7, 1729-1737, 1968.

Garimella, S., Christensen, R.N., Heat Transfer and Pressure Drop Characteristics of Spirally Fluted Annuli: Part I-Hydrodynamics, *ASME Journal of Heat Transfer* 117, 54-60, 1995.

Garimella, S., Christensen, R.N., Heat Transfer and Pressure Drop Characteristics of Spirally Fluted Annuli: Part II-Heat Transfer, *ASME Journal of Heat Transfer* 117, 61-68, 1995.

Heikal, M.R.F., Walklate, P.J. and Hatton, A.P. The Effect of Free Stream Turbulence Level in The Flow and Heat Transfer in the Entrance Region of An Annulus. *Int. J. Heat Mass Transfer* 20, 763-771, 1977.

Hsieh, S.S., Lin, C.C., An Experimental Study of Laminar Entrance Flow and Heat Transfer in Finned Tube Annuli, *Int. J. Heat Mass Transfer* 36, 2457-2471, 1993.

Kahalerras, H., Targui,N., Numerical Analysis of Heat Transfer Enhancement in a Double Pipe Heat Exchanger With Porous Fins, *International Journal of Numerical Methods for Heat & Fluid Flow* 18(5), 593-617, 2008.

Kakaç, S., Shah, R.K., Aung, W., *Handbook of Single-Phase Convective Heat Transfer* , A Willey-Interscience Publication, New York, 1987.

KERN *Teilkristalline Thermoplaste und ihre Eigenschaften, Germany, 1995.*

Kuvvet, K., *Flow and Heat Transfer In Internally Finned Concentric Passage*, PhD. Thesis, Karadeniz Technical University, Turkey, 2002.

Mon,M.S., Gross,U., Numerical Study of Fin-Spacing Effects in Annular Finned Tube Heat Exchangers, *Int. J. Heat Mass Transfer* 47, 1953–1964, 2004.

Patankar, S.V., Ivanovic, M.,Sparrow, E.M., Analysis of Turbulent Flow and Heat Transfer in Internally Finned Tubes and Annuli, *J. Heat Transfer* 101, 29-37, 1979.

Renzoni, P., Prakash, C., Analysis of Laminar Flow and Heat Transfer in the Entrance Region of an Internally

Finned Concentric Circular Annular Duct, *ASME Journal of Heat Transfer*, 109, 532-538, 1987.

Shim, S.Y., Soliman, H.M., Sims, G.E., Turbulent Fluid Flow, Heat Transfer and Onset of Nucleate Boiling in Annular Finned Passages, *Int.J. Thermal Science* 39, 709-720, 2000.

Syed, K. S., Iqbal, M., Mir, N. A., Convective Heat Transfer in The Thermal Entrance Region of Finned Double-Pipe, *Heat Mass Transfer* 43, 449–457, 2007.

Wierzbowski, M., Stasiek ,J., Liquid Crystal Technique Application for Heat Transfer Investigation in a Fin-Fube Heat Exchanger Element, *Experimental Thermal and Fluid Science* 26, 319-323, 2002.

Kemal KUVVET is working as an assistant professor at Gümüşhane University, Gümüşhane, Turkey. He was born in Trabzon-Turkey in 1972. He graduated from the Mechanical Engineering Department of Karadeniz Technical University. He received his Ph.D. degrees from Karedeniz Technical University. His research interests involve numerical heat transfer and fluid flow, heat transfer enhancement, fluid mechanics, experimental methods in the heat and fluid flow. He has several article and project in Turkey and abroad.

Tahir YAVUZ is working as Prof at Başkent University, department of Mechanical Engineering. He was born in Trabzon-Turkey in 1950. He graduated from the Mechanical Engineering Department of Karadeniz Technical University. He received Ph.D. degrees from the Aeronautical Engineering of University of Leicester. He has research about vortex dynamics, boundary layer development, fluid mechanics, heat transfer, thermodynamics and related areas. He has several article and project in Turkey and abroad.